Journal of Marine Research, 58, 709–719, 2000

Theoretical calculations based on real topography of the maximum deep-water flow through the Jungfern Passage

by Karin Borenäs[1] and Anna Nikolopoulos[2]

ABSTRACT

A method for theoretically calculating the maximum transport through a strait, using the actual topography, is presented. The study is conducted within the framework of rotating hydraulics. The results are used for estimating the amount of North Atlantic Deep Water flowing through the Jungfern Passage into the Caribbean Sea. These appraisals are compared with previous theoretical estimates, for which a rectangular bottom profile has been used, and with transport calculations based on observations.

1. Introduction

There are a number of places in the world ocean where deep water is transported from one basin to another through constrictions. These passages play an important role in the deep water circulation, and to provide estimates of the associated fluxes is hence of great importance. Using the theory of rotating hydraulics to determine the maximum flow rates through passages of this type has proven to be convenient. An extensive inventory of different strait and sill flows was recently presented by Whitehead (1998), who calculated the maximum transport through various straits using the zero potential vorticity approximation and furthermore assuming a rectangular cross section. Borenäs and Lundberg (1988) showed that for the Faroe Bank Channel this geometry tends to overestimate the transport compared to when a more realistic parabolic bottom profile is used. There are, however, other straits with a bottom topography for which neither the rectangular nor the parabolic shape is representative. When modeling the flow rate through these contractions it would be desirable to represent the bottom topography in a more adequate manner.

A new technique for theoretically calculating the maximum transport through straits using the real topography is presented in what follows. The calculations are based on rotating hydraulic theory together with the zero potential vorticity approximation. This approach is chosen in order to facilitate a comparison between the present results and earlier estimates for which a rectangular cross section was used. Furthermore, for strait

1. Earth Sciences Centre, Department of Oceanography, Göteborg University, Box 460, SE-405 30 Göteborg, Sweden. ***email: kabo@oce.gu.se***

2. Department of Meteorology/Physical Oceanography, Stockholm University, SE 106 91 Stockholm, Sweden.

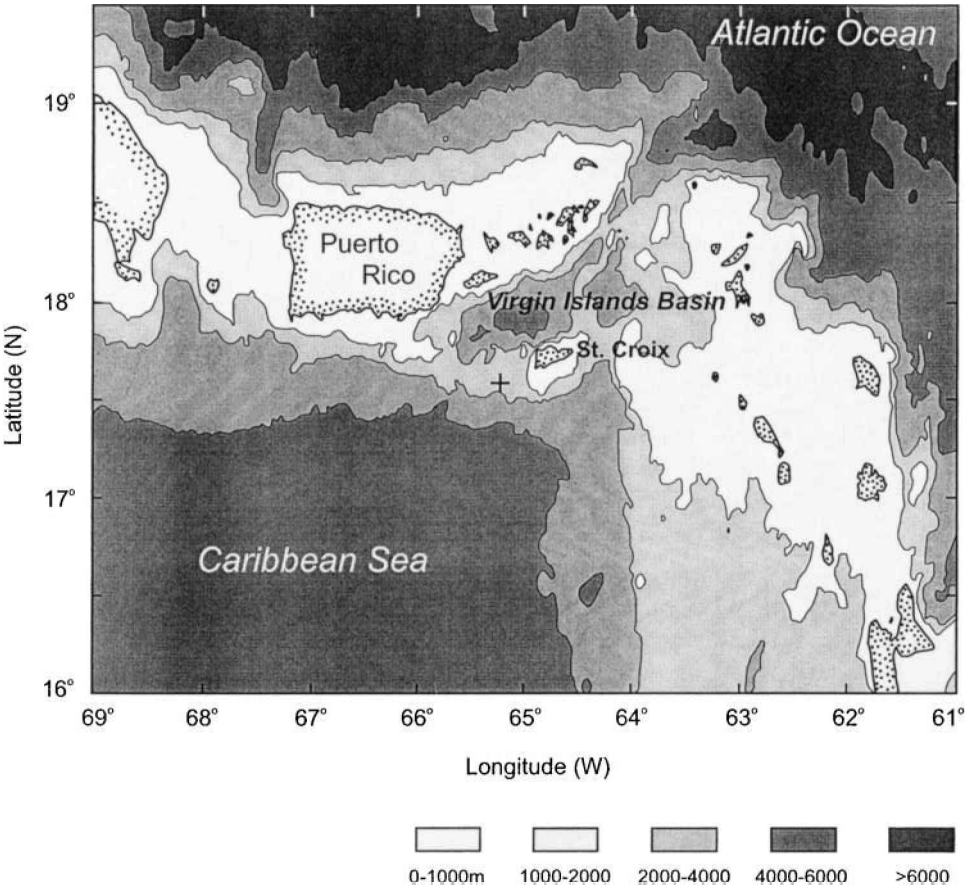

Figure 1. Map showing the bathymetry in the area of the Jungfern Passage. The cross indicates the location of the sill.

widths smaller than or approximately equal to the Rossby radius of deformation, the results from this approximation are usually close to those obtained for a constant potential vorticity flow (cf. Borenäs and Pratt, 1994).

As an example for the calculations, the flow of North Atlantic Deep Water through the Jungfern Passage into the Caribbean Sea is considered (Fig. 1). This passage was recently subjected to a detailed field survey by Fratantoni *et al.* (1997), and a new bathymetry of the strait was presented. As seen in Figure 2, the sill topography is characterized by an elevation in the middle, dividing the channel into a shallow as well as a deeper part, the latter with a sill depth of 1815 m. This hydrographic cross-section (adopted from Fratantoni, 1997) shows a stratified bottom layer consisting of North Atlantic Deep Water, with potential temperatures less than 4°C, in both subchannels. The aim of the present study is to theoretically estimate the maximum transport of this dense water using the actual topography of the strait.

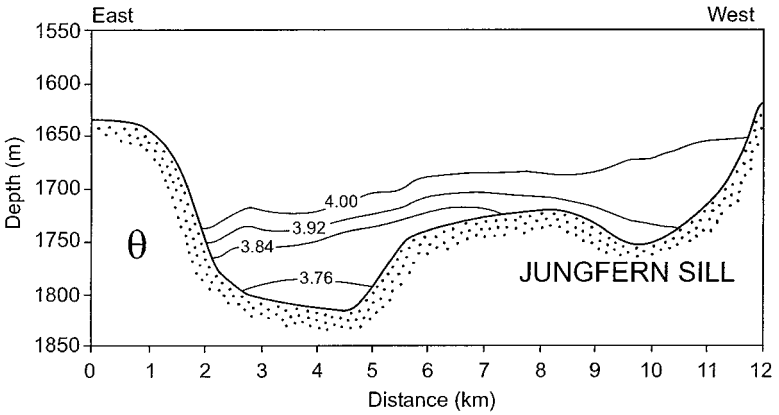

Figure 2. Section showing the potential temperature across the deeper parts of the Jungfern Passage on March 13, 1992 (adopted from Fratantoni *et al.*, 1997).

In the next section the governing equations are presented, and in Section 3 the solution method is outlined and applied to the deep-water flow through the Jungfern Passage. In a concluding section the results are compared with previous estimates and a summary of the general outcome of this study is given.

2. The governing equations

Consider a flow, of constant density ρ, through a strait with an arbitrary cross-sectional topography as shown in Figure 3. This flow takes place beneath a deep, quiescent layer of density $\rho - \Delta\rho$. The coordinate system is prescribed with its origin at the deepest point on

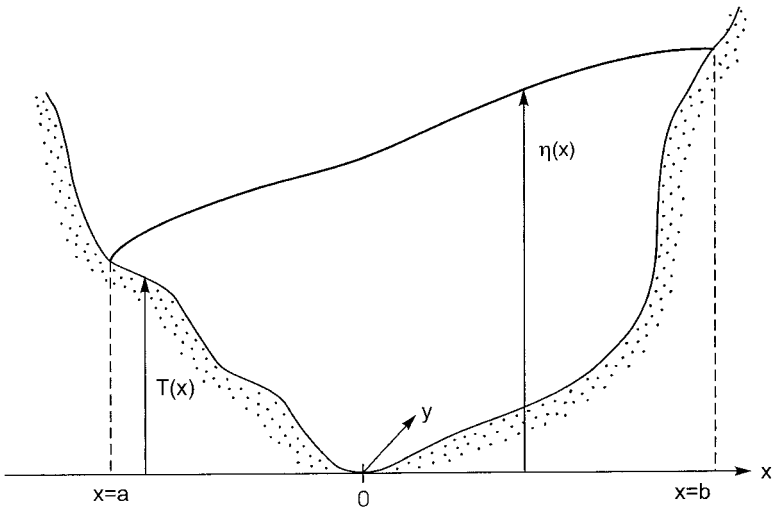

Figure 3. Geometrical variable notation pertaining to a channel with an arbitrary bottom topography.

the sill. If the topography varies slowly in the y-direction, the downstream component of an inviscid flow may be regarded as being in approximate geostrophic balance. The governing equations are then given by

$$vf = g' \frac{\partial \eta}{\partial x}, \tag{1}$$

$$u \frac{\partial v}{\partial x} + v \frac{\partial v}{\partial y} + fu = -g' \frac{\partial \eta}{\partial y}, \tag{2}$$

$$\frac{\partial}{\partial x}(uD) + \frac{\partial}{\partial y}(vD) = 0, \tag{3}$$

where the velocity components in the x and y direction are u and v, respectively, and f is the Coriolis parameter. The height of the interface is $\eta(x)$, the depth of the lower layer is $D(x)$, and the height of the topography is prescribed as $T(x)$. The reduced gravity is defined as $g' = g\Delta\rho/\rho$. From the equations above the potential vorticity equation may be derived, ultimately yielding

$$\frac{f + \partial v/\partial x}{D} = G(\psi), \tag{4}$$

where ψ is the streamfunction. The zero potential vorticity approximation is now made by assuming that $G(\psi) = 0$. The vorticity equation may be combined with Eq. (1) to obtain an equation for the interface:

$$\frac{\partial^2 \eta}{\partial x^2} = -\frac{f^2}{g'},$$

with the general solution

$$\eta = -\frac{f^2 x^2}{2g'} + \frac{fV_0}{g'} x + \eta_0. \tag{5}$$

The solution involves two constants to be determined; V_0, the velocity at $x = 0$, and η_0, the height of the interface at $x = 0$. It turns out, though, to be more convenient to express V_0 and η_0 in terms of the as yet undetermined variables a and b. This may be accomplished by noting that the depth equals zero at these end-points. Since $D(x) = \eta(x) - T(x)$ the following identities are obtained:

$$D(a) = -\frac{f^2 a^2}{2g'} + \frac{fV_0 a}{g'} - T(a) + \eta_0 = 0, \tag{6a}$$

$$D(b) = -\frac{f^2 b^2}{2g'} + \frac{fV_0 b}{g'} - T(b) + \eta_0 = 0. \tag{6b}$$

Expressions (6a, b) may be combined to yield

$$V_0 = \frac{f}{2}(b-a) + \frac{(T(b)-T(a))g'}{f(b+a)} \tag{7}$$

and

$$\eta_0 = \frac{f^2}{8g'}[(b+a)^2-(b-a)^2] - \frac{(b-a)}{2(b+a)}[T(b)-T(a)] + \frac{1}{2}[T(b)+T(a)]. \tag{8}$$

One relation between a and b is obtained by applying the Bernoulli function, $B(\psi)$, along either boundary. This function is related to the potential vorticity by $G(\psi) = dB/d\psi$, and is, in the case of $G(\psi) = 0$, a constant. Hence, the Bernoulli equation assumes the following form:

$$\tfrac{1}{2}\, v^2 + g'\eta = g'\eta_\infty, \tag{9}$$

where η_∞ is the height of the interface in the upstream basin where the velocities are presumed to be small. By inserting the values of v and η at e.g. $x = a$, the following expression is obtained:

$$\frac{[T(b)-T(a)]^2 g'^2}{2(b+a)^2 f^2} + \frac{f^2}{8}(b+a)^2 + \frac{g'}{2}[T(b)+T(a)] = g'\eta_\infty. \tag{10}$$

The second relationship between a and b is given by specifying the volume flux

$$Q = \int_a^b vD\,dx = \frac{g'}{2f}[\eta^2(b)-\eta^2(a)] - \int_a^b vT\,dx. \tag{11}$$

In the next section, Eqs. (10) and (11) will be used for calculating the maximum flow through the strait.

3. The solution method applied to the deep-water flow through the Jungfern Passage

The first step is to determine all possible combinations of a and b which satisfy Eq. (10) for a given upstream height η_∞. This is done by prescribing a (with the associated bottom height $T(a)$), and then solving (10) for all b subject to the constraint that $T(b) > T(a)$, this to ensure that the net transport is positive. The procedure is repeated for all a such that the bottom height $T(a)$ is less than η_∞, which is the largest conceivable value of η. (The last property may formally be shown by determining the x for which the identity $\partial\eta/\partial x = 0$ is satisfied. This value of x is inserted in Eq. (5) and by using the expressions given in (7), (8), and (9), it may be demonstrated that $\eta_{\max} = \eta_\infty$.) As will be seen, there may be other restrictions which also have to be taken into account. Once the permissible range of a has been established, all the possible combinations of a and b may be determined.

Hereafter the transports associated with the admissible *a*-*b* pairs are calculated from Eq. (11). The first term on the right-hand side is immediately available, whereas the integral must be evaluated using standard numerical methods. A relation between Q and a (or b) is hence established, from which the maximum flow capacity of the strait is given.

This procedure is now applied to the Jungfern Passage and the example to be discussed here pertains to the situation shown in Figure 2. Apart from knowing the topography at the sill, one needs a value for the upstream height of the interface, η_∞, as well as g'. These values will be taken from the observations in the area due to Fratantoni *et al.* (1997).

The transport of dense water with potential temperature <4°C will be determined for all permissible configurations of the interface. Since no upstream observations were reported by Fratantoni *et al.* (1997), the largest height of the 4°C isotherm at the cross-section here shown is instead chosen as the upstream value of the interface, i.e. $\eta_\infty = 165$ m. The reason for not choosing a higher upstream value is partly based on the observations presented by Stalcup *et al.* (1975), who reported upstream heights in the range of 100–150 m, but is also due to theoretical considerations. In the case of a parabolic cross-section Borenäs and Lundberg (1988) found that if the channel is equal to or wider than the Rossby radius of deformation there exists a streamline for which the upstream height is preserved along the channel. The Jungfern Passage is somewhat larger than the Rossby radius (based on the upstream height) for values of η_∞ up to around 250 m. Going beyond this value of η_∞, calculations show that the maximum height of the interface at the sill will finally be lower than the upstream height, but it will still be far too high than the value observed. Considering these results, η_∞ is hence chosen to be the same as the maximum height of the interface at the sill, i.e. 165 m. The value of g' is further taken to be 4.5×10^{-4} m/s^2 (determined from the observations presented by Fratantoni *et al.,* 1997) and $f = 0.45 \times 10^{-4}$ s^{-1}.

The combinations of a and b, which satisfy Eq. (10), are hereafter calculated and the results are shown in Figure 4. As mentioned above, only solutions for which $T(b) > T(a)$ are taken into account, and hence certain areas in the *a*-*b* space are excluded. (These regions are hatched in the figure.) The solutions associated with the upstream height $\eta_\infty = 165$ m are shown as two solid curves where the thin segments indicate nonpermitted combinations of a and b representing solutions which, as will be shown, are not connected.

The cross-stream position of the interface is shown in Figure 5 for four *a*-*b* pairs. The special examples to be considered here are indicated in Figure 4 by A, B, C, and D, respectively. For case A the flow extends across the entire passage. Case C represents a flow in the shallow subchannel, whereas for case D the flow is found only in the deeper part of the passage. Figure 5 also demonstrates that the unphysical solution B (represented by the broken curve) is not connected between the end-points a and b.

The transport Q may now be calculated, in terms of a, for all permissible pairs of a and b and the results for $\eta_\infty = 165$ m are presented in Figure 6 as solid curves. From this graph it is possible to determine the maximum transport through the passage. In Figures 4 and 6 the solution and transport curves are also shown for $\eta_\infty = 120$ m, 90 m, and 60 m, this in order to illustrate the effect of a lowered interface. (The value of g' is kept the same.) It is obvious

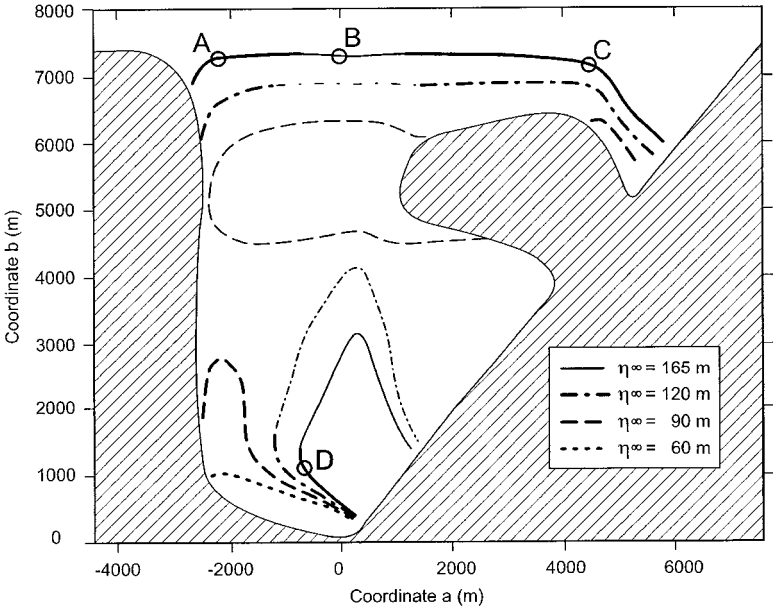

Figure 4. Coordinate pairs which are solutions to Eq. (10) for different upstream heights. The hatched areas are nonpermissible since they represent negative net flows. The thin curves, or the thin parts of the curves, indicate nonconnected solutions and are hence also excluded. For solutions A, B, C, and D the associated interface shapes across the Passage are shown in Figure 5.

that the flow rate is very sensitive to changes of the upstream height. For instance, a change of η_∞ from 60 m to 120 m increases the maximum transport by a factor of four.

4. Results and discussion

The inflow of North Atlantic Deep Water through the Anegada-Jungfern Passage has previously been estimated on a number of occasions. Stalcup *et al.* (1975) gave an

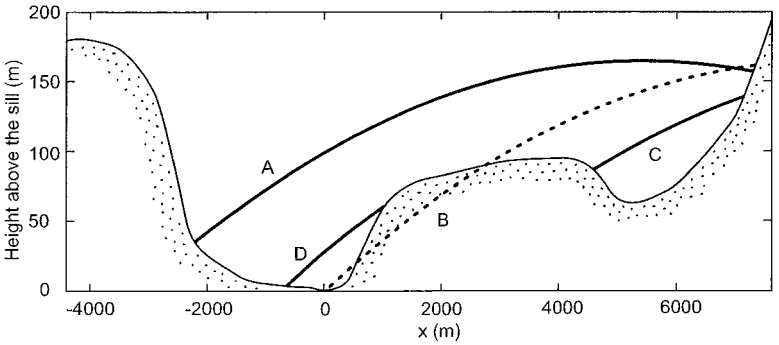

Figure 5. Four examples (based on solutions A, B, C and D in Fig. 4) showing different configurations of the interface across the passage when the upstream height is given by η_∞ = 165 m. The B curve is not a permitted solution since the end-points are not connected.

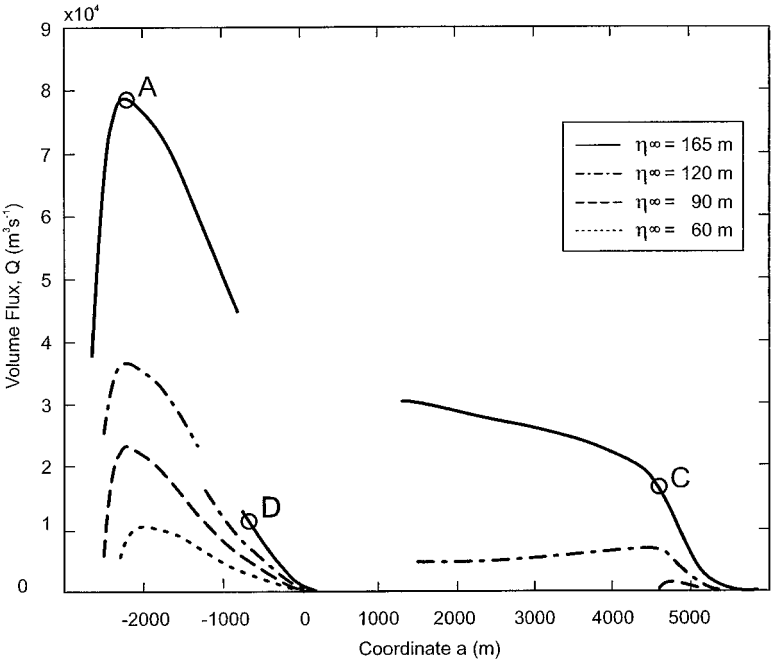

Figure 6. The flow rate through the Passage, given as a function of the end-point, a, for various upstream heights of the interface. The circles indicate the values corresponding to solutions A, C and D in Figure 4.

appraisal of the deep-water transport based on hydrography and current meter measurements. These authors also employed the hydraulic approach introduced by Whitehead *et al.* (1974) in order to calculate the maximum transport through the Jungfern Passage. The area was recently subjected to renewed investigations by Fratantoni *et al.* (1997) and MacCready *et al.* (1999). The latter authors calculated a mean value of the transport through the Jungfern Passage based on 14 months of ADCP measurements and thermistor chain records in the passage. Fratantoni *et al.* (1997), on the other hand, estimated the deep-water flux at one special occasion, using more detailed observations of the hydrography and velocity structure across the Jungfern Passage. The results obtained in the course of the present investigation will be discussed and compared with these previous transport calculations.

In Section 3 the solutions for a flow of potential temperature $<4°C$, and with an upstream height of 165 m, were discussed and the cross-channel structure was given for some specific cases. Example A corresponds to the solution of maximum transport of water below the 4°C isotherm (as demonstrated in Fig. 6) yielding $Q_{max} = 0.79 \times 10^5$ m^3/s. The average velocity of this flow can also be calculated, giving $\overline{v} = 0.12$ m/s. It is evident from Figure 5 that the interface associated with case A indicates a reversed flow on the right-hand side of the passage (looking in the downstream direction). This is due to the fact

that for a flow of zero potential vorticity the theoretical shape of the interface is a fixed parabola. If the channel is wider than the Rossby radius of deformation, the maximum height of the parabola is found somewhere within the channel, hence giving rise to negative velocities adjacent to the right-hand channel boundary. In the theoretical work by Killworth (1994) it was demonstrated that a region with flow reversals on the right-hand side can be replaced by an area of quiescent water, thereby increasing the net flux. This region will extend from the point were $\partial\eta/\partial x = 0$ (corresponding to $v = 0$) and continue to the right hand boundary. Hence, if only the positive part of the flow is considered here, the transport increases somewhat to 0.85×10^5 m^3/s.

The theoretical values above should be compared with the flow rate obtained when the area under the 4°C isotherm in Figure 2 is multiplied by the mean velocity obtained from the ADCP measurements reported by Fratantoni *et al.* (1997). Taking the average velocity across the passage to be 0.12–0.15 m/s, the transport will range between 0.72 and 0.90×10^5 m^3/s. The present theoretical results are in good agreement with the observational estimates on this particular occasion. Had a rectangular cross section been considered in the theoretical calculations instead of the real topography, the maximum flow rate had become 1.36×10^5 m^3/s. The calculated transport reported by Fratantoni *et al.* (1997), based on the same observations used here, was 1.6×10^5 m^3/s, which is larger than both the theoretical and the empirical estimates presented above. Since these authors do not present the details on how this transport was calculated, it is difficult to see what causes the discrepancies. It may be interesting here to compare the results with the long-term mean estimates of the flux given by MacCready *et al.* (1999). Their obtained transport was 0.85×10^5 m^3/s, but this value was calculated for water with potential temperature <3.965°C.

In Stalcup *et al.* (1975) the theory of rotating hydraulics was applied to estimate the maximum transport of water with potential temperature < 3.8°C through Jungfern Passage. Calculations were made for two flow situations characterized by upstream heights $\eta_\infty = 100$ m and 150 m, respectively, assuming zero potential vorticity and a rectangular cross section (see Whitehead *et al.,* 1974). In both cases the reduced gravity was taken to be $g' = 4.0 \times 10^{-4}$ m/s^2. The transport formula presented by Whitehead *et al.* (1974) also includes the width of the channel, for which Stalcup *et al.* (1975) used the value 5 km for the lower interface height and 6 km when the interface was higher. With these parameter estimates the inflow of cold Atlantic water was found to be 0.4×10^5 m^3/s and 0.9×10^5 m^3/s, respectively. If (as in the present investigation) the same zero potential vorticity theory is applied using identical parameters as Stalcup *et al.* (1975) but real topography, the maximum inflow becomes 0.27×10^5 m^3/s and 0.55×10^5 m^3/s for the smaller, respective larger, upstream height. As expected (Borenäs and Lundberg, 1988), these transport values are smaller than those obtained by Stalcup *et al.* (1975). The flux estimates based on hydrography and direct current measurements (Stalcup *et al.,* 1975), were 0.56×10^5 m^3/s and 0.99×10^5 m^3/s, for the two situations.

In the review by Whitehead (1998), transport calculations were made for a number of straits and passages using rotating hydraulic theory for a zero potential vorticity flow

through a rectangular cross-section. The maximum transport estimates were compared to calculations based on observations and for all cases reported, the ratios between the theoretical and the observed values were found to be in the range 1.3–2.7. The present study shows that by using real topography, the theoretically calculated values of the maximum flow rate are reduced and should, therefore, conform better to observations. For the dense flow through the Jungfern Passage, the agreement between this theoretical estimate and the empirical one (calculated here from the observations presented by Fratantoni *et al.* (1997)) was good. However, as mentioned above, the estimate made by these authors, using the same data, was much larger. The appraisals, based on observations given by Stalcup *et al.* (1975), also exceed the theoretical values calculated in the present study in which the actual topography has been used. The empirical estimates by both Fratantoni *et al.* (1997) and Stalcup *et al.* (1975) are actually larger than those predicted by the zero potential vorticity theory with a rectangular bottom profile. This is somewhat surprising considering that the "rectangular theory" tends to overestimate rather then underestimate the flow rates.

When discussing maximum flow discharge through constrictions it should be mentioned that Killworth (1994) showed that for an arbitrary but "simple" bottom topography (excluding multiple minima), the zero potential vorticity flow gives the largest possible transport. This result is, however, not immediately applicable to the Jungfern Passage since the bottom topography here does not obey the criterion of being "simple."

Although the calculations in the present study assume steady-state, the actual flows are time-dependent. It is clear that the deep-water flow through the Jungfern Passage is highly variable since the amount of North Atlantic Deep Water in the Virgin Islands Basin shows large fluctuations. Hence, one should avoid applying the stationary hydraulic model during transition periods. According to the time series presented by Stalcup *et al.* (1975), there are, however, periods of 7–10 days when comparatively stationary conditions prevail during which hydraulic theory should be applicable for transport estimates.

Acknowledgments. The work has been supported by the Swedish Natural Science Research Council under contract G-AA/GU 09811-318. The computational method was developed within the EU MAST III VEINS programme MAS3-CT96-0070. The authors would also like to thank Drs. P. Lundberg and L. Pratt for valuable discussions and A. Malm for technical assistance.

REFERENCES

Borenäs, K. and P. Lundberg. 1988. On the deep-water flow through the Faroe Bank Channel. J. Geophys. Res., *93*(C2), 1281–1292.

Borenäs, K. M. and L. J. Pratt. 1994. On the use of rotating hydraulic models. J. Phys. Oceanogr., *24,* 108–123.

Fratantoni, D. M., R. J. Zantopp, W. E. Johns and J. L. Miller. 1997. Updated bathymetry of the Anegada-Jungfern Passage complex and implications for Atlantic inflow to the abyssal Caribbean Sea. J. Mar. Res., *55,* 847–860.

Killworth, P. D. 1994. On reduced-gravity flow through sills. Geophys. Astrophys. Fluid Dyn., *75,* 91–106.

MacCready, P., W. E. Johns, C. G. Rooth, D. M. Fratantoni and R. A. Watlington. 1999. Overflow into the deep Caribbean: Effects of plume variability. J. Geophys. Res., *104*(C11), 25913–25935.

Stalcup, M. C., W. G. Metcalf and R. G. Johnson. 1975. Deep Caribbean inflow through the Anegada-Jungfern Passage. J. Mar. Res., *33,* (Suppl.). 15–35.

Whitehead, J. A. 1998. Topographic control of oceanic flows in deep passages and straits. Rev. Geophys., *36,* 423–440.

Whitehead, J. A., A. Leetmaa and R. A. Knox. 1974. Rotating hydraulics of strait and sill flows. Geophys. Fluid Dyn., *6,* 101–125.

Received: *24 January 2000;* revised: *7 July, 2000.*